Human Molecular Genetics, 2012, Vol. 21, No. 6 **1260–1271**
doi:10.1093/hmg/ddr556
Advance Access published on November 25, 2011

Genomic architecture at the Incontinentia Pigmenti *locus* favours *de novo* pathological alleles through different mechanisms

Francesca Fusco[1], Mariateresa Paciolla[1,2], Federico Napolitano[1], Alessandra Pescatore[1], Irene D'Addario[3], Elodie Bal[4], Maria Brigida Lioi[2], Asma Smahi[4], Maria Giuseppina Miano[1] and Matilde Valeria Ursini[1,*]

[1]Institute of Genetics and Biophysics 'Adriano Buzzati-Traverso', IGB-CNR, Naples 80131, Italy, [2]University of Basilicata, Potenza 85100, Italy, [3]Dermopatic Institute of the 'Immacolata', IRCCS, Rome 00167, Italy and [4]INSERM U781 et Département de Génétique, Hopital Necker-Enfants Malades, Paris 75015, France

Received August 22, 2011; Revised October 13, 2011; Accepted November 22, 2011

***IKBKG/NEMO* gene mutations cause an X-linked, dominant neuroectodermal disorder named Incontinentia Pigmenti (IP). Located at Xq28, *IKBKG/NEMO* has a unique genomic organization, as it is part of a segmental duplication or low copy repeat (LCR1–LCR2, >99% identical) containing the gene and its pseudogene copy (*IKBKGP*). In the opposite direction and outside LCR1, *IKBKG/NEMO* partially overlaps *G6PD*, whose mutations cause a common X-linked human enzymopathy. The two LCRs in the *IKBKG/NEMO locus* are able to recombine through non-allelic homologous recombination producing either a pathological recurrent exon 4–10 *IKBKG/NEMO* deletion (*IKBKGdel*) or benign small copy number variations. We here report that the local high frequency of micro/macro-homologies, tandem repeats and repeat/repetitive sequences make the *IKBKG/NEMO locus* susceptible to novel pathological IP alterations. Indeed, we describe the first two independent instances of inter-*locus* gene conversion, occurring between the two LCRs, that copies the *IKBKGP* pseudogene variants into the functional *IKBKG/NEMO*, causing the *de novo* occurrence of p.Glu390ArgfsX61 and the *IKBKGdel* mutations, respectively. Subsequently, by investigating a group of 20 molecularly unsolved IP subjects using a high-density quantitative polymerase chain reaction assay, we have identified seven unique *de novo* deletions varying from 4.8 to ~115 kb in length. Each deletion removes partially or completely both *IKBKG/NEMO* and the overlapping *G6PD*, thereby uncovering the first deletions disrupting the *G6PD* gene which were found in patients with IP. Interestingly, the 4.8 kb deletion removes the conserved bidirectional promoterB, shared by the two overlapping *IKBKG/NEMO* and *G6PD* genes, leaving intact the alternative *IKBKG/NEMO* unidirectional promoterA. This promoter, although active in the keratinocytes of the basal dermal layer, is down-regulated during late differentiation. Genomic analysis at the breakpoint sites indicated that other mutational forces, such as non-homologous end joining, *Alu-Alu*-mediated recombination and replication-based events, might enhance the vulnerability of the IP *locus* to produce *de novo* pathological IP alleles.**

INTRODUCTION

Incontinentia Pigmenti (IP; OMIM 308300) is a rare X-linked dominant disease, lethal in males, affecting the neuroectodermal tissues, always associated with skin defects. The cutaneous lesions, starting in the neonatal period and naturally evolving in four successive inflammatory stages, are hallmarks for IP diagnosis (1,2).

About 73% of IP females carry a loss-of-function mutation in the *IKBKG/NEMO* gene (inhibitor of kappa light polypeptide

*To whom correspondence should be addressed at: Institute of Genetics and Biophysics 'Adriano Buzzati-Traverso', IGB-CNR, Via P. Castellino, 111, Naples 80131, Italy. Tel: +39 0816132262; Fax: +39 0816132706; Email: ursini@igb.cnr.it

gene enhancer in B-cells, kinase gamma/nuclear factor kappaB, essential modulator, GenBank NM_003639.3, OMIM 300248), whereas in 27% of cases the mutation still remains elusive (3). The *IKBKG/NEMO* gene encodes for NEMO/IKKgamma which acts as a regulatory subunit of the inhibitor of the kappaB (IkB) kinase (IKK) complex required for canonical nuclear factor kappaB (NF-kappaB) pathway activation involved in many fundamental physiological functions (4,5). It is currently believed that the highly heterogeneous and often severe clinical presentation of IP might be due to the pleiotropic role of the NEMO/IKKgamma. In addition, the absence of NEMO/IKKgamma protein makes the cells sensitive to apoptosis, leading to the IP-associated male lethality and skewed X-inactivation in females (6–10). The *IKBKG/NEMO locus* has a unique genomic organization. In the centromeric direction, the *IKBKG/NEMO* gene partially overlaps the *G6PD* (glucose-6-phosphate dehydrogenase, GenBank NM_000402) gene. The two overlapping genes share a conserved promoter region (promoterB), which has a housekeeping bidirectional activity (11–13). It is worth nothing that *G6PD* is a disease gene, causing the X-linked *G6PD* deficiency (OMIM 305900) (14), the most common enzymopathy in humans. More then 140 different hypomorphic mutations of *G6PD* have been identified so far, whereas large deletions or a loss-of-function mutation of this gene have never been discovered, leading geneticists to consider that the absence of this gene might be lethal in males (15–17).

In the telomeric direction, the *IKBKG/NEMO* gene is part of a 35.7 kb segmental duplication containing two low copy repeats (LCRs) arranged in an opposite orientation, one covering the functional gene (LCR1) and the other its partial pseudogene copy (LCR2).

IKBKG/NEMO is structured in nine coding exons (exons 2–10) and four alternative non-coding first exons. Transcription from exons 1B and 1C is directed by the strong bidirectional promoterB, whereas that from exons 1D and 1A is directed by a weak unidirectional promoterA, located in intron 2 of *G6PD* (13). The non-functional *IKBKGP* spans the region between exons 3 and 10.

A recurrent deletion (*IKBKGdel*) frequently associated with IP (>70% of cases) is generated by non-allelic homologous recombination (NAHR) due to a misalignment between two MEdium Reiterated 67B (*MER67B*) repeated sequences. The deletion removes a region, ~11.7 kb in length, spanning exons 4–10 in the *IKBKG/NEMO* gene. Furthermore, the NAHR mechanism can also generate benign copy number variations (CNVs), such as the exon4–10 *IKBKGP* deletion, named *IKBKGPdel*, and the exon4–10 *IKBKG/NEMO* gene duplication, named *MER67Bdup*, that are both risk alleles for pathological *IKBKGdel* in IP patients. Notably, 65% of IP cases are sporadic carrying a *de novo IKBKG/NEMO* mutation (18,19).

The LCR1 and LCR2 sequence homology makes them prone to recombination, as extensively documented in previous reports. Aradhya *et al*. (18) detected evidence for sequence exchange between the LCR1 and LCR2 copies pointing out that inversion events promoted by their opposite orientation might be responsible for the maintenance of their similarity.

More recently, we have observed that recombination events produced by NAHR between the two LCRs repositioned an exon4–10del from the pseudogene to the *IKBKG/NEMO* gene, thereby causing the IP pathogenic mutations (19). Finally, recent papers have provided additional proof showing that recombination between these two LCRs might cause the copy number gain observed in mental retardation families (20,21).

We here report that the high frequency of micro/macrohomologies, tandem repeats and repeat/repetitive sequences might predispose the IP *locus* to novel types of genomic rearrangements arising through different mechanisms generating pathological alterations (22). We report the first instances of *IKBKG/NEMO* pathogenic mutations resulting from gene-conversion events and arising between the two homologous LCRs. Furthermore, using a custom-designed high-density quantitative real-time polymerase chain reaction (qRT-PCR) in a group of molecularly unsolved IP patients, we have identified seven different deletions involving not only *IKBKG/NEMO*, but also the overlapping *G6PD* gene or, in one case, eliminating the bidirectional promoterB. The analysis of such a promoterB deletion has revealed novel unsuspected features of the regulatory region of the *IKBKG/NEMO* gene, which may explain the manifestation of the skin defects in the carrier patient.

RESULTS

Gene conversion mediated by LCRs in the IP *locus* causes a *de novo* mutation in the *IKBKG/NEMO* gene

A mechanism such as inter- or intra-chromatid unidirectional gene conversion might be expected to generate pathological alterations in the IP *locus* because of the high degree of homology between the two LCRs (>99% identity). Supporting this assumption, we identified two unrelated IP families in which a sequence variation in *IKBKGP* in the unaffected father was unidirectionally copied in *IKBKG/NEMO* by a gene-conversion event causing the disease in the affected daughter.

In the IP-603 family, the proband (Fig. 1A, II:1) carried a known c.1167delC mutation in *IKBKG/NEMO* exon 10, leading to the frameshift p.Glu390ArgfsX61 in the NEMO/IKKgamma protein (3) and the non-pathogenic c.1167delC in its *IKBKGP* pseudogene (Fig. 1B). The unaffected father (Fig. 1A, I:2) carried the c.1167delC in the *IKBKGP* pseudogene (Fig. 1B).

Genotype analysis of the family members performed using five polymorphic microsatellites [short tandem repeats (STRs)] surrounding the IP *locus* (DXS1684, DXS8061, DXS15, DXS1073 and DXS1108) did not identify any recombination event and revealed that the proband inherited the X chromosomes matching the relative haplotype asset present in each parent (Fig. 1A). Therefore, c.1167delC is located in the inherited paternal allele, suggesting that a gene-conversion event had occurred during paternal meiosis.

In the second family, IP-583 (Fig. 2A), we investigated a sporadic IP case (Fig. 2A, III:1) carrying the common pathological *IKBKGdel* and also two non-pathogenic CNVs, *IKBKGPdel* and *MER67Bdup* (Figs. 2A and B and 3A). To assess the mechanism generating the occurrence of the *IKBKGdel*, we studied the inheritance of both CNVs in IP-583 relatives and we observed the presence of the

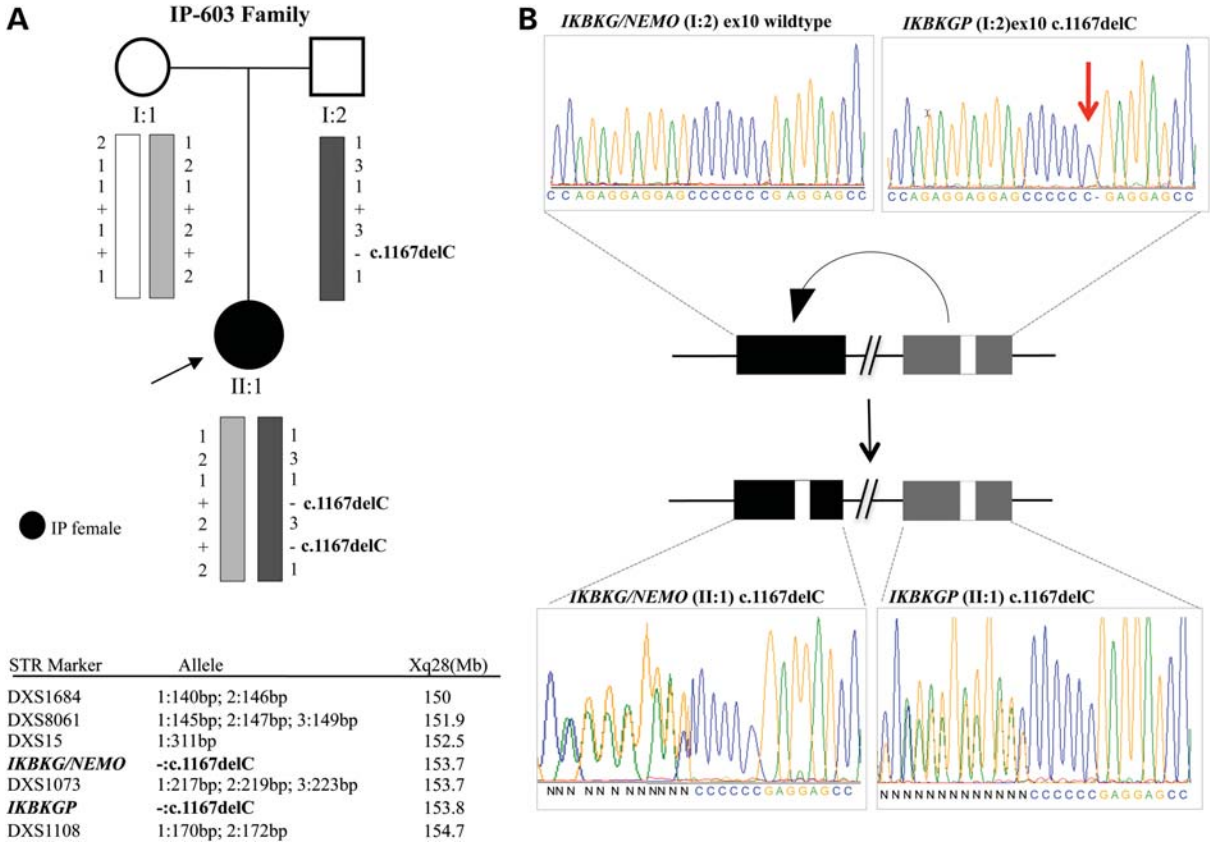

STR Marker	Allele	Xq28(Mb)
DXS1684	1:140bp; 2:146bp	150
DXS8061	1:145bp; 2:147bp; 3:149bp	151.9
DXS15	1:311bp	152.5
IKBKG/NEMO	**-:c.1167delC**	153.7
DXS1073	1:217bp; 2:219bp; 3:223bp	153.7
IKBKGP	**-:c.1167delC**	153.8
DXS1108	1:170bp; 2:172bp	154.7

Figure 1. IP-603 family analysis reveals a gene-conversion event. (**A**) IP-603 pedigree; the affected IP patient (II:1) is indicated by a black symbol. The haplotype analysis by multiallelic STR markers (DXS1684, DXS8061, DXS15, DXS1073 and DXS1108) at the *IKBKG/NEMO locus* in the IP-603 family is shown. (**B**) Sequence analysis of exon10 in the *IKBKG/NEMO* gene and in the *IKBKGP* pseudogene. On the top, the electropherograms of exon10 in the gene (wild-type) and in the pseudogene (mutation c.1167delC, chrX:delG_153 868 348–153 868 349) in the IP-603 father (I:2) are shown; on the bottom, the electropherograms of the point mutation c.1167delC, p.Glu390ArgfsX61 observed in the IP-603 patient (II:1) in the *IKBKG/NEMO* gene and in the *IKBKGP* pseudogene are shown. The model of the gene conversion is shown.

IKBKGPdel in the father (II:2, Fig. 2A and B) and the *MER67Bdup* in the unaffected mother (II:1) and grandmother (I:2, Fig. 2A and B). STR analysis along the female lineage of the IP proband (III:1) revealed the presence of *MER67Bdup* in the recombinant N2 haplotype, indicating that this duplication is located in the *IKBKG/NEMO* gene of the maternal allele (Fig. 2A). Consequently, the pathological *IKBKGdel* is located in the paternal haplotype (N5), suggesting that a gene-conversion event is the most obvious mechanism able to explain the presence of the exon 4–10 deletion in both the pseudogene and the gene in the proband. This may have occurred between the *IKBKGPdel* and the wild-type *IKBKG/NEMO* gene in the father's germline homogenizing the gene and pseudogene sequences and making both mutated.

Novel deletions in the IP *locus* involve *IKBKG/NEMO* and overlapping genes

Mutations of the *IKBKG/NEMO* gene are responsible for 70–80% of IP. The lack of *IKBKG/NEMO* mutations in the remaining 20–30% of IP cases is probably due to the detection system. For this reason, we decided to test 20 patients, with an unambiguous clinical diagnosis of IP (based on skin biopsy analysis) but lacking molecular diagnosis, by using a custom-designed high-density quantitative real-time polymerase chain reaction (qRT-PCR), which proved to be effective in revealing quantitative DNA alterations in the IP *locus*.

We designed 13 specific primer pairs (Ps): 9 able to amplify fragments with a single localization (PF, P1, P2, P3, P4, P9, P10, P11 and P12; Fig. 3B) covering the region from the *G6PD* to *CTAG2* (Cancer/Testis AntiGen 2, NM_020994, OMIM 300396; Fig. 3B) genes, outside the LCRs; and 4 (P5, P6, P7 and P8) with a double localization, in LCR1 and LCR2 (Fig. 3B, Supplementary Material, Fig. S1A) (19). As a control, we established the genomic profile of the PF to P12 probe in 10 control DNA female samples (XX) and 10 male samples (XY). No apparent alteration in the 13 IP samples was observed, whereas an abnormal RT-PCR genomic profile, found in seven samples (IP-48, IP-51, IP-11, IP-47, IP-50, IP-14 and IP-43), indicated the presence of different size deletions (Supplementary Material, Fig. S1B and Table S1). In IP-48, both LCR1 and LCR2 were deleted. Indeed, the probes localized in the duplicated region were calculated to have two fewer copies. In the other six IP samples, the quantification probes indicated only the presence of LCR2, whereas in IP-43 two intact LCRs were counted (Fig. 3C, Supplementary Material, Table S1). Thus, we identified seven deletions in heterozygotes of different lengths,

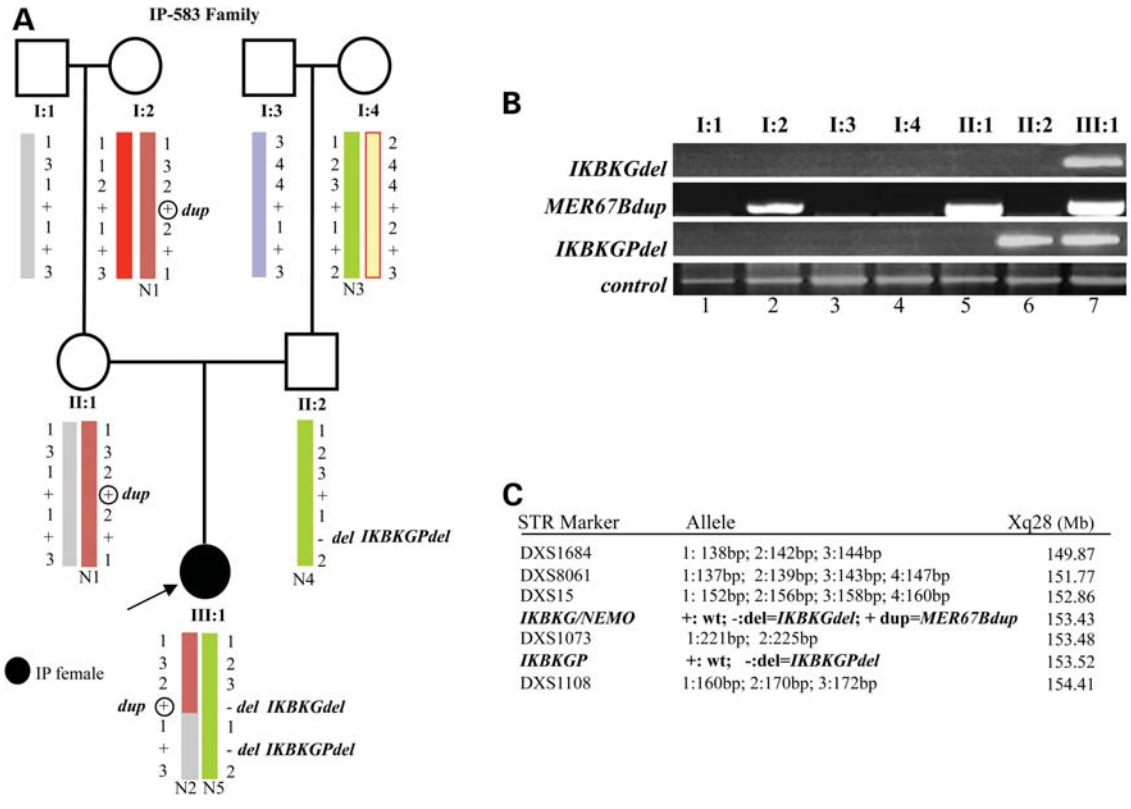

Figure 2. IP-583 family analysis reveals a gene-conversion event. (**A**) IP-583 pedigree; the affected IP patient (III:1) is indicated by a black symbol. The haplotype analysis by multiallelic STR markers (DXS1684, DXS8061, DXS15, DXS1073 and DXS1108) at the *IKBKG/NEMO locus* in the IP-583 family is reported. N1 and N2 represent the haplotypes that segregate through the female lineage of the IP proband (III:1), whereas N3, N4 and N5 segregate through the male lineage of III:1. N1 and N2 carried the *MER67Bdup* (*dup*), whereas N4 and N5 carried the exon4–10 deletion *IKBKGPdel* (*del*) in the pseudogene. N5 also carried the deletion *IKBKGdel* (*del*) in the gene. (**B**) PCR tests in the IP-583 family reveal the presence of *IKBKGdel* in III:1; *MER67Bdup* in I:2, II:1 and III:1; and *IKBKGPdel* in II:2 and III:1. (**C**) STR legend.

each including both *IKBKG/NEMO* and the overlapping *G6PD* genes. To map the breakpoints, we designed additional primers in the 5′ (proximal) and 3′ (distal) sequences flanking the deleted regions (Supplementary Material, Tables S2 and S3). Surprisingly, although the distal junctions (3′_IP) of the seven deletions mapped in different positions within the *locus*, the proximal junctions (5′_IP) were clustered in two regions that we called R1 and R2 (Fig. 3B). In IP-48 and IP-51, the 5′-breakpoint (5′-bkp) was predicted to be in a region located in *G6PD* intron5 (R1 region, Fig. 3B, Supplementary Material, Table S2), whereas in IP-11 and IP-47, the 5′-bkp was predicted to be in *G6PD* 3′ untranslated region (UTR; R1 region, Fig. 3B, Supplementary Material, Table S2). In IP-14 and IP-43, the 5′-bkp was proximal to *G6PD* exon2 (R2 region, Fig. 3B, Supplementary Material, Table S2), whereas in IP-50 it was in *G6PD* intron2 (R2 region, Fig. 3B, Supplementary Material, Table S2). The 3′-bkp positions were unique and scattered along LCR1 with the exception of IP-48 and IP-43 whose 3′-bkp positions were located outside LCR1 and LCR2. In IP-48, the 3′-bkp mapped in the region between *IKBKGP* and *CTAG2*, whereas in IP-43 the distal breakpoint mapped in the region between *IKBKG/NEMO* intron1C and intron2 (Fig. 3B, Supplementary Material, Table S3).

The genomic architecture flanking the breakpoint junctions reveals a local high content of repeat elements

To explore why the *IKBKG/NEMO locus* and the surrounding genomic regions are prone to rearrangement, it was essential to determine the positions of the breakpoint-clustering regions and to analyse the junction-sequence signatures in detail. Therefore, we performed an *in silico* analysis of the IP *locus* to search for repeat sequences potentially able to lead to genomic instability (23–30).

The tandem repeats finder (31) showed that the highest number of tandem elements was found to be located in LCR1 and LCR2 (chrX:153 790–153 800 kb and chrX:153 860–153 870 kb; UCSC Genome Browser on Human Feb. 2009 GRCh37/hg19; Supplementary Material, Table S4) as well as in the region upstream of the *IKBKG/NEMO* gene (chrX:153 750–153 760 kb; Supplementary Material, Table S4).

Repeated sequence analysis, performed by Repeated Mask, revealed an enrichment of short interspersed element (SINE) repeat elements (*Alu* sequences) in the region proximal to LCR1 (chrX:153 740–153 780 kb), of long-interspersed elements (LINEs) in the region near LCR2 (chrX:153 880–153 900 kb) and of long terminal repeats (LTRs) between LCR1 and LCR2 (chrX:153 820–153 840 kb; Supplementary

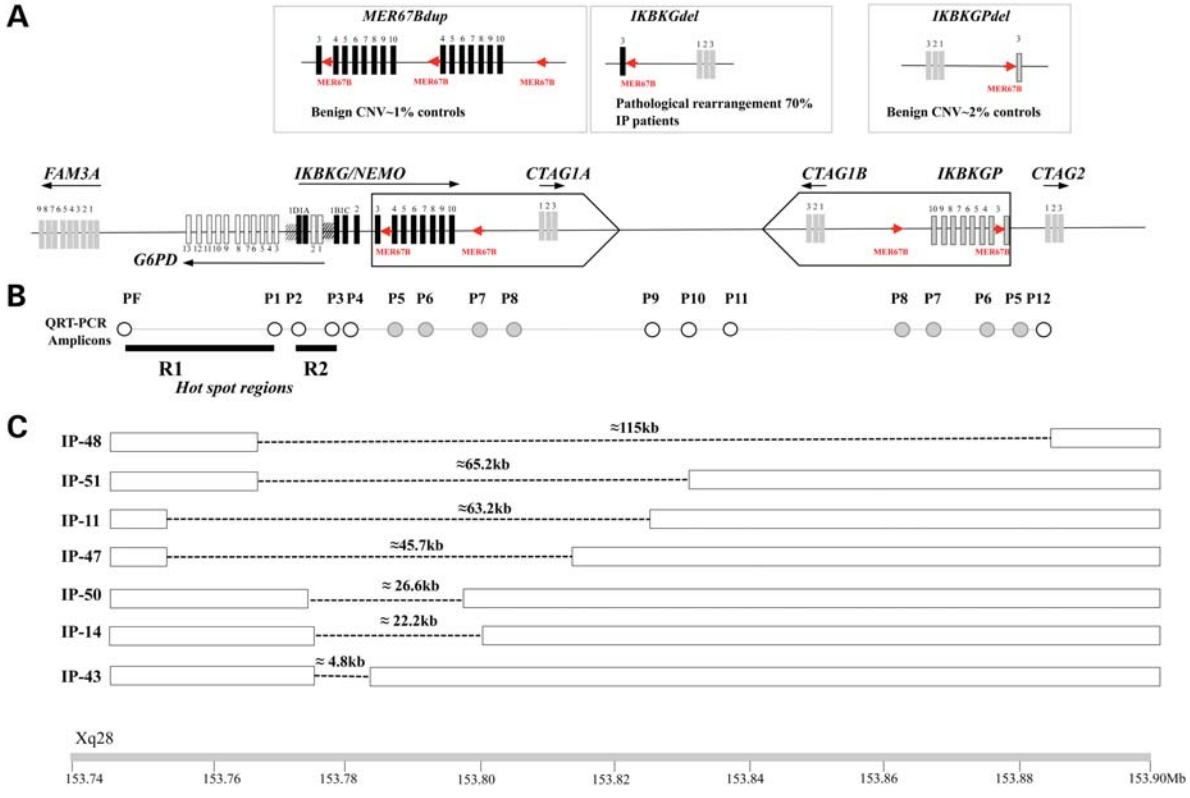

Figure 3. IP *locus* comprehensive map of novel genomic rearrangements. (**A**) Recurrent rearrangements in the IP *locus*. Schematic representation of benign CNVs (*MER67Bdup* and *IKBKGPdel*) and the pathogenic *IKBKGdel* deletion produced by NAHR. The frequency of each rearrangement is reported. Genomic structure of the IP *locus* in Xq28 (chrX:153 740–153 900 kb, UCSC Genome Browser on Human February 2009, GRCh37/hg19). The square arrows represent LCRs. The *FAM3A* (OMIM 300492) exons (grey boxes), *G6PD* exons (empty boxes), *IKBKG/NEMO* exons (black boxes), *IKBKGP* exons (grey boxes) and *CTAG1A/B*, *CTAG2* exons (grey boxes) are shown. The arrows indicate the transcriptional direction for each gene. The red arrows indicate the *MER67B* repeated sequences. (**B**) The qRT-PCR amplicons are shown. PF, P1, P2, P3, P4, P9, P10, P11 and P12 (open circles) have a single localization, whereas P5, P6, P7 and P8 (filled circles) have a double localization. The R1 (chrX:153 747 962–153 763 394 bp, 15 432 bp) and R2 (chrX:153 769 022–153 774 414 bp, 5392 bp) 'hot spot' (boxed) regions are shown. (**C**) Schematic view of the deleted regions in the IP patients. The dotted lines show the localization and size of the novel rearrangements associated with IP. The deletion extension was calculated by measuring the distance between the two probes with an altered copy number.

Material, Table S4) and near LCR2 (chrX:153 880–153 900 kb; Supplementary Material, Table S4).

Taken together, these observations reveal that the breakpoint 'hot spots' clustered in R1 (chrX:153 740–153 770 kb) and R2 (chrX:153 760–153 780 kb) were in regions with a high content of SINEs (33% in R1 and 28.9% in R2) and tandem repeat elements (24 and 7% in R1 and R2, respectively) but with a low content of LINEs (4.2% in R1 and 14.1% in R2) and LTRs (5.8% in R1 and 6.2% in R2) (Supplementary Material, Table S4). On the contrary, an enrichment of specific repetitive sequences was not observed within the genomic region surrounding the 3′ junctions (Supplementary Material, Table S4). One exception was noticed in the chrX:153 810–153 820 kb region where the 3′_IP-11 breakpoint was in 41.6% of the LTR sequences (Supplementary Material, Table S4). In the 3′-bkp of IP-14 and in the IP-50 (3′_IP-14, 3′_IP-50) samples, we found a high number of tandem repeat elements (chrX:153 790–153 800 kb; Supplementary Material, Table S4).

Finally, we looked for sequence homologies (23–30) in a 10 kb region surrounding the 5′ and 3′ breakpoint junctions in each IP sample. We found that the 11 breakpoint regions were located in *AluS* elements (four *AluScs*, two *AluSxs*, two *AluSgs*, two *AluSq2s* and one *AluSz*), and *AluYs* and *AluJbs* (Table 1). More interestingly, their junction regions appeared to contain microhomology sequences (16–118 bp in length) (Table 1).

Fine mapping of the breakpoint junctions in the IP-43 sample defines the novel *IKBKGdelB* IP allele

The determination of the junction sequences, although it represents a key point in the study of the origin of rearrangements, is not always easy to obtain in the case of large alterations (30), especially where a high sequence complexity surrounds the breakpoints making it very difficult to sequence them. This is the case in our study in which the breakpoint deletions are located in regions with a high content of DNA repeats and, consequently, we were not able to identify the precise break junctions except for the rearrangement found in the IP-43 sample. Indeed, we used different nested primer pairs to narrow down the deleted region observed in the IP samples but we obtained the informative amplicon only in IP-43 (Supplementary Material, Fig. S2). In this case, we amplified a fragment of 5.8 kb in the control DNA and a fragment of 1.0 kb in the IP sample (primers B–E; Supplementary

Table 1. List of IP patients and their observed breakpoints in the IP *locus*

ID	Origin	Minimal deletion size (bp)[a]	Upstream X-chromosomal position	Downstream X-chromosomal position	Deleted region	Extended homology	Micro-homology
IP-48	Italian	11 5198	153 763 394	153 878 592	*G6PD* exons 1–4, *IKBKG/NEMO*, *CTAG1A*, *CTAG1B*, *IKBKGP*	*AluJb*(241 bp)/*AluY* (290): 84%	16 bp (95%)
IP-51	Greek	65 249	153 763 394	153 828 643	*G6PD* exons 1–4, *IKBKG/NEMO*, *CTAG1A*	*AluSg* (261 bp)/*AluY* (298 bp): 88%	70 bp (75%)
IP-11	Italian	63 275	153 757 815	153 821 090	*G6PD*, *IKBKG/NEMO*, *CTAG1A*	*AluSx* (292 bp)/*AluSz* (315 bp): 75%	57 bp (85%)
IP-47	Spanish	45 745	153 757 815	153 803 560	*G6PD*, *IKBKG/NEMO*	*AluSx* (226 bp)/*AluSg* (264 bp): 86%	16 bp (95%)
IP-50	Mexican	26 568	153 769 487	153 796 055	*G6PD* exons 1 and 2, *IKBKG/NEMO*	*AluSc5* (382 bp)/*AluSq2* (441 bp): 87%	90 bp (85%)
IP-14	French	22 218	153 774 414	153 796 632	*G6PD* exons 1 and 2, *IKBKG/NEMO*	*AluSc5* (382 bp)/*AluSq2* (441 bp): 87%	48 bp (95%)
IP-43	Spanish	∼4 800[b]	153 774 414	153 776 269	*G6PD* exons 1 and 2, *IKBKG/NEMO* exon1B-1C	*AluSc* (258 bp)/*AluSc* (299 bp): 86%	118 bp (85%)

All IP patients showed a severe IP phenotype (seizures and mental retardation) but IP-43 had only skin IP alterations.
All IP patients were extremely skewed for the X-inactivation pattern in peripheral blood lymphocytes (X-inactivation values ≥90:10%) and in IP-43 also in the skin biopsy.
[a]The deletion extension was calculated by measuring the distance (bp) between the two probes with an altered copy number in the qRT-PCR experiments.
[b]In IP-43, the size of the deletion resulting from the PCR amplification is reported.

Material, Fig. S2). This was the smallest fragment obtained in the IP DNA suggesting the presence of a deletion of about 4.8 kb in IP-43 (Supplementary Material, Fig. S2).

Nucleotide sequence analysis of this fragment (B–E, Supplementary Material, Fig. S2) validated the positional mapping of the deletion but did not allow us to sequence across the breakpoint junctions. Indeed, both the proximal (5′-bkp segment; Fig. 4A and Supplementary Material, Fig. S2A) and distal (3′-bkp segment; Fig. 4A and Supplementary Material, Fig. S2A) breakpoints were located in high-density contiguous *Alu* elements (88.70 and 85.45% of *Alu*, respectively; Fig. 4B). This architecture suggested that an *Alu-Alu*-mediated recombination had occurred in the IP-43 progenitor germline. Two homology regions (HR1 and HR2) were present in 5′-bkp (HR1) and 3′-bkp (HR2) with 86% of identity (Supplementary Material, Fig. S3). In addition, the 5′-bkp contained two long tandem repeats [(TTTTG)n (TTTT)n, TR in Fig. 4B] making it impossible to sequence their junction fragments.

IKBKGdelB deletion abolishes the promoterB that regulates *IKBKG/NEMO* expression in keratinocyte differentiation

The 4.8 kb deletion detected in the IP-43 sample removed the 5′ UTR end portion of the *IKBKG/NEMO* gene (covering the non-coding 1B and 1C exons) and the 5′ region of *G6PD* (covering exons 1 and 2) (Fig. 4A). We have named this novel deletion *IKBKGdelB*, because it eliminates the entire *IKBKG/NEMO* promoterB, leaving intact the *IKBKG/NEMO* exon 2 that contains the ATG. The *IKBKGdelB* allele in the IP-43 patient would be expected to lack the transcription driven by promoterB, leaving only the mRNA transcribed from promoterA. We have previously shown that the *IKBKG/NEMO* promoters A and B act independently (13). Nevertheless, in the skin of the IP-43 patient, who presented only the characteristic dermatosis (Table 1), we did not know whether promoterA was functioning. Indeed, any further analysis of the *in vivo* expression of the *IKBKGdelB* allele was denied by the skewed X-inactivation profile (>90:10%) observed in the IP-43 DNA skin biopsy. We previously reported (13) that promoterA directs transcription from the alternative exon 1D (liver-specific) and 1A isoforms, whereas promoterB directs the transcription from the 1B and 1C isoforms (Fig. 5A). To obtain a better insight into the contributions of the promoterA- and promoterB-directed transcriptions in the skin, we analysed their activity by RT-PCR in two conditions: (i) *in vivo* on RNA from different layers of the skin from healthy donors (Fig. 5B) and (ii) *in vitro* on RNA from differentiated and proliferating HaCat keratinocyte cell lines (Fig. 5C). By using primer pairs, specific for each *IKBKG/NEMO* isoform, we discovered that although 1C was not expressed, 1A was reduced during keratinocyte differentiation and only the 1B transcript expression was consistently present. Therefore, promoterA was functioning in the lower undifferentiated layers of the skin and was down-regulated during the differentiation, whereas promoterB was expressed in all layers of the skin (Fig. 5B). Comparable results were obtained in the *in vitro* differentiated HaCat keratinocyte cell line (Fig. 5C). In both systems, we determined the expression of *DeltaNp63alfa*, as a marker of skin differentiation (Fig. 5B and C). Moreover, the level of expression of *G6PD* did not change during keratinocyte differentiation (data not shown).

DISCUSSION

We have previously reported that the IP *locus* can undergo NAHR producing either pathological rearrangements (*IKBKG-del*) or benign variants (*MER67Bdup* and *IKBKGPdel*) (19). In this study, we highlight that other molecular mechanisms, such as gene conversion, Non-Homologous End-Joining (NHEJ), Microhomology-Mediated End Joining (MMEJ) and Fork

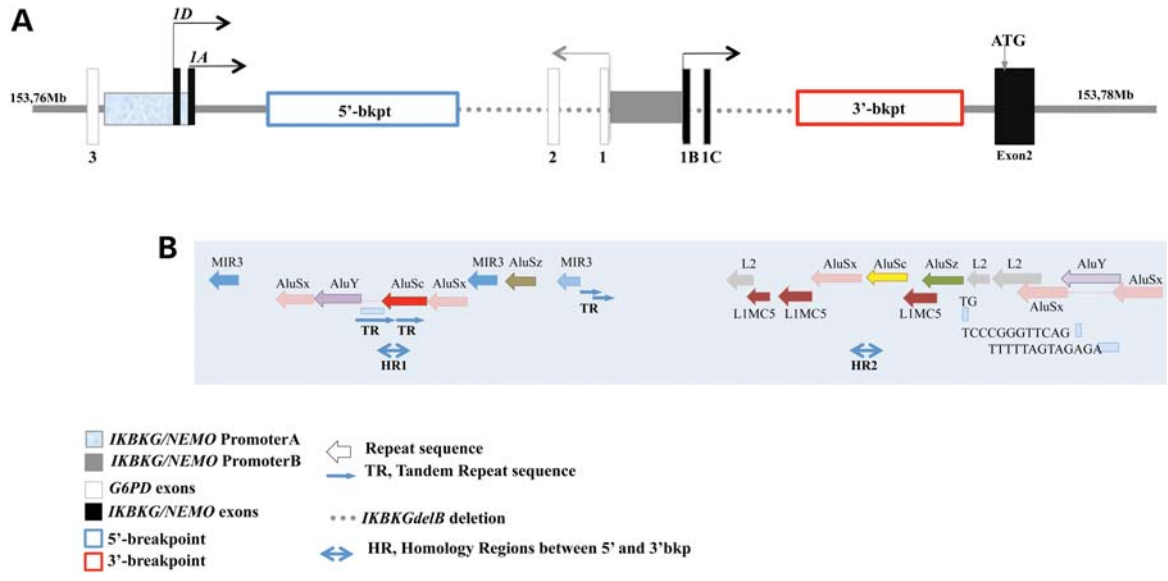

Figure 4. Repeated sequence analysis around the 5′-bkp and 3′-bkp junctions of the *IKBKGdelB* deletion. (**A**) Schematic representation of the *IKBKGdelB* deletion. The horizontal arrows show the transcription direction. The *IKBKG/NEMO* non-coding exons (1D, 1A, 1B and 1C) and *G6PD* exons 1 and 2 are shown. (**B**) The filled arrows represent the repeated sequences. TR, tandem repeat.

Stalling and Template Switching (FoSTeS), may take place at the IP *locus*. We have discovered novel IP mutations generated by *de novo* events during parental gametogenesis whose origin could be due to the peculiar genomic architecture of the *IKBKG/NEMO* region. Most of them are novel rearrangements whose breakpoint site analysis reveals the disruption of the overlapping *G6PD* gene and of one of the *IKBKG/NEMO* regulatory elements that is controlled during skin development.

Different mechanisms operate in the IP *locus* enhance the vulnerability of *IKBKG/NEMO* to mutations

Gene conversion, the non-reciprocal exchange of genetic information between homologous DNA sequences, could be implicated in the IP disease. On the basis of haplotype analyses, we here report an intrachromatid gene-conversion event that may occur during paternal spermiogenesis. These findings were obtained by studying two unrelated families with two sporadic IP females carrying *de novo IKBKG/NEMO* mutations: the mutations identified in the functional *IKBKG/NEMO* are copied from the *IKBKGP* pseudogene. In both cases, the father had a pseudogene polymorphism (c.1167delC in IP-603 I:2; *IKBKGPdel* in IP-583 II:2, Figs 1 and 2) that perfectly matched the mutation identified in the gene in the affected daughters.

In general, gene conversion cannot be formally distinguished from double crossover (32) and, therefore, we cannot exclude the possibility that a NAHR event between misaligned chromatids had occurred in the probands' parental germlines. However, the replacement of the wild-type sequence with a mutated sequence (c.1167delC or *IKBKGdel*) in the gene acceptor, copying it from a highly homologous sequence in the pseudogene donor, is an extremely likely event when compared with the occurrence of an identical *de novo* alteration. It is worth noting that, gene-conversion events producing sequence identity between the *IKBKG/NEMO* gene and its pseudogene have already been reported by Aradhya *et al*. (18), but instances of gene-conversion mutations generating the pathological *IKBKG/NEMO* allele have not been reported until now. Finally, in the above reported cases, the gene-conversion event occurred in paternal germlines (Figs 1 and 2). It is indeed well known that during spermiogenesis, programmed double-strand breaks (DSBs) are induced to facilitate the chromatin remodelling that takes place in the elongating spermatids (33,34) and that proteins involved in the homologous recombination repair machinery are present (35).

Besides gene-conversion mutations, we provide evidence of other mutational mechanisms facilitated by the local genomic architecture and able to trigger IP alleles as *de novo* rearrangements. We identified seven different *de novo* deletions in heterozygotes which had arisen in a context of high-density repeat sequences and micro/macro-homologies (16–118 bp, Table 1) that are well-known substrates for different mutational forces such as NHEJ, MMEJ and/or FoSTeS (26–28). *In silico* analysis of the DNA sequence at the IP *locus* revealed a high prevalence of repeat sequences, such as SINEs, LINEs and LTRs, especially at the proximal breakpoints (Supplementary Material, Table S4) (36). These repetitive elements, together with tandem repetitive elements, are able to generate DSBs or to provide unusual DNA secondary structures including cruciforms, hairpins, triplexes and tetraplexes (37) that may inhibit DNA polymerization increasing the probability of generating rearrangements. Moreover, all the deletion breakpoints are clustered within or in the proximity of *Alu* repeat clusters (Table 1), frequently involved in recombination events (38–40). In addition, the presence at the breakpoint junctions of microhomologies due to short homologous DNA stretches (16–118 bp, Table 1) makes more likely mechanisms based on coupled homologous and non-homologous recombination, homologous single-strand

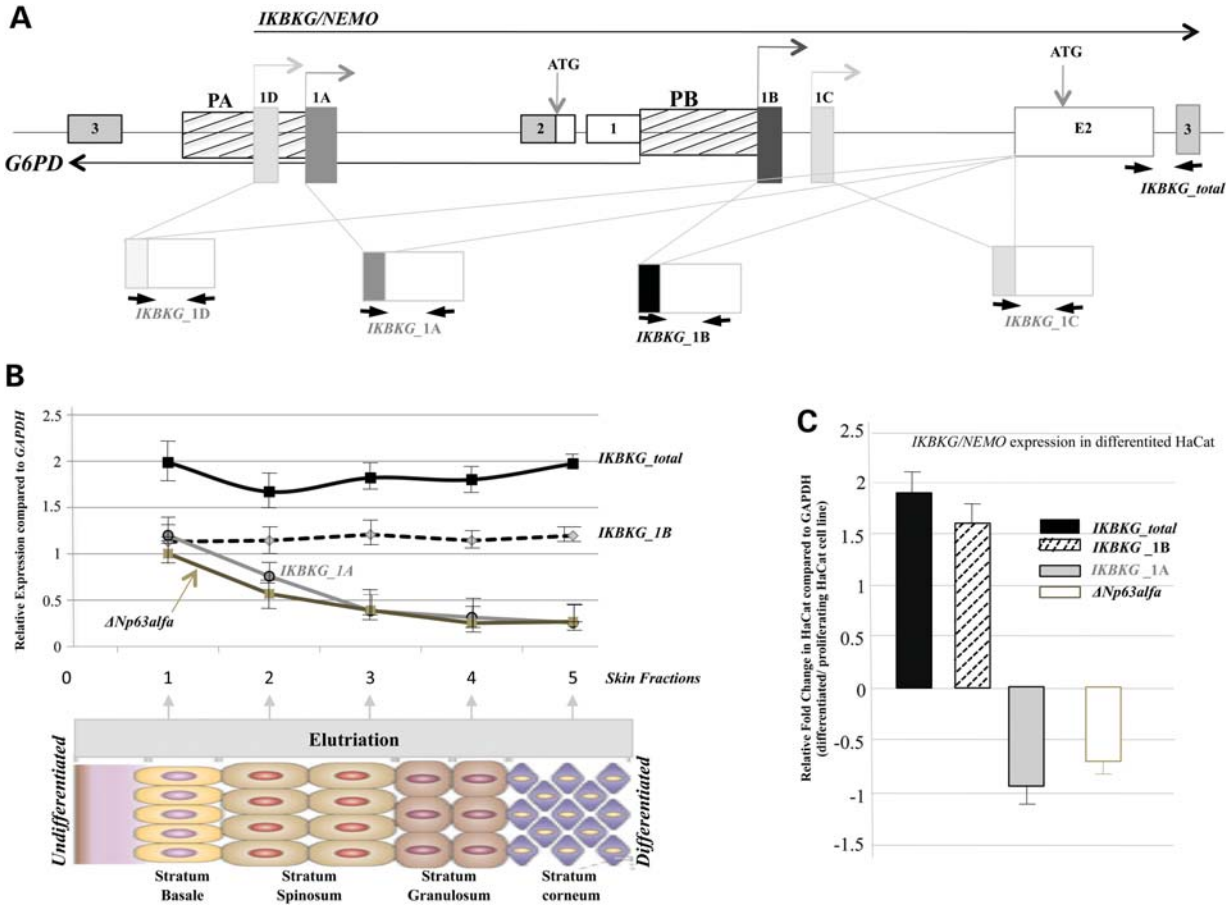

Figure 5. *IKBKG/NEMO* promoter structure and qRT-PCR analysis of the 5′ UTR alternative isoforms in differentiated skin layers. (**A**) Genomic structure of the *IKBKG/NEMO* promoters. PromoterA (PA) is unidirectional and located in *G6PD* intron2, whereas PromoterB (PB) is bidirectional and located between the *G6PD* and *IKBKG/NEMO* genes. The 5′ UTR alternative isoforms (*IKBKG_1D*, *IKBKG_1A*, *IKBKG_1B* and *IKBKG_1C*) of *IKBKG/NEMO* are shown. The arrows indicate the position of the primers used for the RT-PCR experiments. (**B**) Quantification of the *IKBKG/NEMO* transcripts by RT-PCR analysis on cDNA from different layers of the skin, obtained by centrifugal elutriation assay (57). We used primers amplifying from exon 2 to exons 1A, 1B and 1C, respectively, and a primer pair to quantify the *IKBKG*_total transcript, located between exons 2 and 3. The expression profile of the 1B isoform, transcribed from promoterB, shows the same profile as the *IKBKG*_total, suggesting that it accounts for most of the *IKBKG/NEMO* transcripts. More interestingly, the 1A isoform decreases from fraction 1 to fraction 5 suggesting a down-regulation during skin differentiation. (**C**) The quantification of the *IKBKG/NEMO* transcripts in the HaCat keratinocytes during *in vitro* differentiation is reported. *IKBKG_1B* is the more abundant transcript having a stable expression in both the proliferating and differentiated HaCat cell lines. The *IKBKG_1A* transcript is less abundant in the differentiated cells. The isoforms *IKBKG_1D* and *IKBKG_1C* are not expressed in the skin fractions and in the HaCat cell line. The *DNp63alfa* (OMIM 603273) transcript is expressed in the basal layer of the human epidermis and is down-regulated during keratinocyte differentiation (58,59).

invasion and completion by an MMEJ event. On the other hand, all seven rearrangements arise in a genomic context in which the presence of LCRs might drive the DSBs (41–43) or might stimulate genomic rearrangements without being physically involved, as in the FoSTeS model (44).

Large deletions of *IKBKG/NEMO* found in IP patients extend to overlapping genes

Besides the recurrent intragenic *IKBKG/NEMO* exon 4–10 deletion described in most IP cases, *IKBKGdel*, we report here seven novel large deletions affecting *IKBKG/NEMO* and the centromeric and telomeric located genes, *G6PD* and *CTAG1A/B*, respectively. Each deletion had a proximal junction in the *G6PD* gene deleting from 3′ UTR to exon 1 (Fig. 3C and Table 1). The genomic organization of the IP *locus* in the centromeric direction shows that the *IKBKG/NEMO* and *G6PD* genes are overlapping and divergently transcribed from opposite strands of the DNA in a ‘head-to-head’ organization conserved during evolution (12,13).

The *G6PD* gene encodes for the initial enzyme of the pentose phosphate pathway (14). Glucose-6-phosphate dehydrogenase deficiency, an X-linked disease, is the most common human enzyme defect. The patients, most frequently males, exhibit non-immune haemolytic anaemia in response to stress or fava bean ingestion. Heterozygous female carriers of a *G6PD*-deficient allele may present clinical manifestations of G6PD deficiency, i.e. favism and severe chronic haemolytic anaemia (45), although, in most cases, they have almost normal G6PD levels due to a selective advantage of cells expressing the normal allele (17).

The *G6PD* gene exhibits a remarkable polymorphism in human populations (>400 variants) and almost all mutations are point alterations resulting in amino acid substitutions

(15,17,46), whereas large deletions or loss of function of this gene have never been discovered. Data from the *g6pd*(−) mouse embryo suggest that alleles with rearrangements deleterious for the *G6PD* gene are embryonic lethal, whereas heterozygous carrier female mice may survive due to the strong selection against mutant cells early in haematopoiesis (47). The results obtained in mice are partially in agreement with the results obtained in women who are heterozygous for certain severe human *G6PD* mutations who present a drastic skewed X-inactivation essentially confined to the blood (46). However, males carrying the same mutation in hemizygotes may survive although presenting severe haemolytic anaemia.

On the other hand, an extensive skewing of X-inactivation has commonly been observed in the blood and fibroblasts of IP patients as indeed a skewed X-inactivation has been considered a diagnostic criterion of IP before undergoing genetic diagnosis (1,48).

Our study is the first to report large deletions involving the *G6PD* gene in IP patients. The patients here described did not present any clinical manifestations matching the classic *G6PD* deficiency leading us to hypothesize that a somatic progressive selection against cells expressing the mutated alleles may occur. Therefore, the deleted *IKBKG/NEMO* allele is able to trigger IP outcomes in the carrier females, whereas the *G6PD* deleted allele is silent because selection masks the G6PD deficiency outcome in the haematopoietic cells.

Finally, the *CTAG1A* (OMIM 300657) and its identical copy *CTAG1B* (OMIM 300156) genes are located in Xq28, LCR1 and LCR2 (18). *CTAG1A/B* cancer/testis antigens genes, which were deleted in three out of seven IP patients (IP-48, IP-51, IP-11), are expressed in a variety of malignant tumours but solely in the testis among normal adult tissues (49). Therefore, no additional abnormalities of the IP phenotype due to the contribution of the deletion of the *CTAG1A/B* genes should be observed in those patients.

Functional relevance of the *IKBKGdelB* deletion for the *IKBKG/NEMO* expression in the keratinocytes

The discovery of the first IP rearrangement involving one of the key regulatory elements of *IKBKG/NEMO* expression gives us an entry point to investigate the *IKBKG/NEMO* gene transcription regulation. We have already established that *IKBKG/NEMO* has two main conserved regulatory regions: promoterB is a strong bidirectional promoter which directs transcription from exons 1B and 1C, whereas promoterA is a weak unidirectional promoter, located in intron 2 of *G6PD* that directs transcription from exons 1D and 1A (13). In the IP-43 patient, we mapped a genomic deletion (*IKBKGdelB*) of the bidirectional promoterB. The deletion abolished the exons *IKBKG_1B*, *IKBKG_1C*, *G6PD*_exon1 and *G6PD*_exon2 that are promoterB-dependent, whereas the *IKBKG/NEMO* translational start site, located in exon 2, was not affected.

The absence of promoterB would result in a severe form of the disease in IP-43, and the patient instead presented only the classic IP skin alterations. The higher degree of X-inactivation skewing which we measured in the peripheral blood and in the skin biopsy of the patient precluded the expression analysis *in vivo* and suggested a strong disadvantage for cells expressing the *IKBKGdelB* which would disappear preferentially after X-inactivation. The coordinated regulation of two *IKBKG/NEMO* promoters offers a model to explain the skin lesion pathogenesis in the IP-43 patient. Indeed, the patient's keratinocytes expressing the *IKBKGdelB* allele in the basal layer of the skin could contain the NEMO/IKKgamma protein translated only from the 1A isoform. During keratinocyte differentiation, the physiological decline of the 1A isoform and the lack of 1B synergically contribute to deplete those cells of the *IKBKG/NEMO* transcripts, to inhibit the NF-kappaB signalling and to cause premature keratinocyte death by apoptosis. According to the model of IP skin pathogenesis, the spontaneous necrotic cell death of some NEMO-deficient keratinocytes triggers the expression of proinflammatory mediators by the neighbouring wild-type keratinocytes resulting in the development of the skin lesions (50,51).

Conclusions

The presence of highly homologous regions (LCR1 and LCR2) and the high density of repetitive sequences may have a genome structure-destabilizing effect and predispose the IP *locus* to generate novel rearrangements by different mechanisms. The result of these rearrangements are non-redundant pathological alleles whose analysis has unravelled the existence of a large deletion of the *G6PD* gene but also novel unsuspected regulatory mechanisms of *IKBKG/NEMO* gene transcription regulation that could be more intricate than previously thought. Taken together, our results lead us to propose that IP belongs to the class of pathological condition also known as genomic disorders (52).

MATERIALS AND METHODS

Subjects

All the IP patients analysed in this study met the 1993 revised criteria for the classification of IP (1,2). All patients' material was gathered, after receiving the informed consent from the participants, under protocols approved by the Declaration of Helsinki. Each potential participant with IP was interviewed and asked to complete an extensive questionnaire. All medical records of IP-affected family members were reviewed to confirm the diagnosis. All affected females underwent skin biopsy obtained from the limbs, usually from the legs. The cutaneous lesions (erythema, vesicles and pustules in the first stage, followed by verrucous and keratotic lesions in the second stage, linear hyperpigmentation in the third stage and pale, hairless, scarring patches in the fourth stage) were observed in all patients. The results of the skin biopsies led unequivocally to a diagnosis of IP.

Blood samples were collected in ethylenediaminetetraacetic acid tubes, and genomic DNA was extracted using the conventional salt precipitation technique. All patients had an apparently normal karyotype. The subjects were initially screened by the following conventional assays (9,19): the *IKBKG/NEMO* gene deletion (*IKBKGdel*) and *IKBKGP* pseudogene deletion were investigated by a long-range PCR with the EXPAND Long Template PCR system (Roche, Mannheim, Germany) as described in Bardaro *et al*. (53). For point mutation screening of coding sequences, the electropherograms

were obtained by direct sequencing using Big Dye Terminator Cycle Sequencing Reactions on an ABI 3100 (PE Applied Biosystems, Lennik, Belgium) on a PCR fragment of each exon and were compared with the genomic sequences from GenBank and from control samples.

STR microsatellite analyses and qRT-PCR

Five microsatellite markers distributed along the Xq28 IP region (DXS1684, DXS8061, DXS15, DXS1073 and DXS1108) were genotyped in the families under study. We used in this analysis all the polymorphic STR markers available in the region, as described in public databases (UCSC, Ensembl, etc.) and also additional dinucleotide repeats developed and characterized in the Xq28 region as previously described (54). We identified and delimited the unrepeated regions in chrX:153 747 962–153 959 172 by RepeatMask, and we designed six primer pairs for real-time experiments outside the duplicated region, as described in Fusco *et al*. (19). All amplification products (70–100 bp) were mapped in the unrepeated regions and were interspersed at 3–20 kb of sequence intervals (PF-P1, 15.4 kb; P1–P2, 5.6 kb; P2–P3, 5.4 kb; P3–P4, 1.4 kb; P9–P10, 7.5 kb; P10–P11, 2.3 kb; P11–P12, 47.6 kb; P12–P13, 7.2 kb). RT-PCR assays were carried out on the Applied Biosystems (Lennik, Belgium) 7900HT system by using the interaction of SYBR Green as a fluorescent reporter (Power SYBR Green PCR Master Mix, Applied Biosystems). The primers, designed using Primer express 3.0 oligo software (Applied Biosystems), are available upon request. All quantifications were normalized to the endogenous gene control *Beta-2-microglobulin* (*B2M* gene, GenBank NM_004048.2; OMIM 109700). A total of 25 ng of genomic DNA (in triplicate) from each sample was subjected to RT-PCR experiments using the specific synthetic primers. The DNA copy number was determined as 2E-ddCt for a patient versus a female control, as described in Fusco *et al*. (19).

Long-range PCR amplification

Oligonucleotide real-time data were used to initially pinpoint approximate breakpoint positions in the genome. We next designed primers for deletions to amplify the rearrangement breakpoint junctions. Different orientations and combinations of primers were also tested for breakpoint analyses. Long-range PCR was conducted with TaKaRa LA Taq polymerase according to the manufacturer's protocol.

Cell culture and centrifugal elutriation and *in vitro* differentiation assays

Human keratinocytes were grown to confluence as described (55,56), trypsinized and collected by centrifugation. The cells were fractionated according to cell size by methods described earlier (57).

For *in vitro* differentiation assays, HaCaT cells were grown in 0.1% foetal calf serum, and $CaCl_2$ was added to a final concentration of 1.2 mM. The cells were harvested at 0 and 6 days after calcium induction.

Gene expression analysis by qRT-PCR

Human total RNA from an undifferentiated keratinocyte cell line and at different stages of differentiation was used as a source of cDNA. Reverse transcription was carried out with the Superscript III enzyme (Invitrogen, Life Technologies, Carlsbad, CA) according to the manufacturer's protocol. The *IKBKG/NEMO* 5′ UTR variants and the overall expression of *IKBKG/NEMO* were detected using primers described in Fusco *et al*. (13). qRT-PCR assays were carried out on the Applied Biosystems 7900HT system by using the interaction of SYBR Green as a fluorescent reporter (Power SYBR Green PCR Master Mix, Applied Biosystems). An automatically calculated melting point dissociation curve generated after every assay was examined to ensure the presence of a single PCR species and the lack of primer–dimer formation in each sample. Standard curves were generated from serial 1/5 dilutions of cDNA. The corresponding RT-PCR efficiency was calculated for each couple of primers. The normalized gene expression was calculated as described in Fusco *et al*. (13).

ONLINE RESOURCES

Online Mendelian Inheritance in Man (OMIM): http://www.ncbi.nlm.nih.gov/Omim/.

UCSC Genome Browser: http://genome.ucsc.edu/index.html?org=Human.

NCBI Reference Sequence (RefSeq): http://www.ncbi.nlm.nih.gov/RefSeq/.

Tandem Repeats Finder: http://tandem.bu.edu/trf/trf.html.

RepeatMasker: http://www.repeatmasker.org/.

Basic Local Alignment Search Tool: http://blast.ncbi.nlm.nih.gov/.

EMBL Nucleotide Sequence Database: http://www.ebi.ac.uk/embl/.

SUPPLEMENTARY MATERIAL

Supplementary Material is available at *HMG* online.

ACKNOWLEDGEMENTS

The authors thank the patients and their families, the physicians, the International Incontinentia Pigmenti Foundation (http://imgen.bcm.tmc.edu/IPIF/) and Association Incontinentia Pigmenti France (http://www.incontinentiapigmenti.fr) for contributing to this research study. We wish to acknowledge Stefania Filosa for helpful discussions.

Conflict of Interest statement. None declared.

FUNDING

This work was supported by TELETHON (grant GGP08125) to M.V.U., by Association Incontinentia Pigmenti France (http://www.incontinentiapigmenti.fr) fellowship to A.P. and to E.B. and by Programme Hospitalier de Recherches Clinique (PHRC) to A.S.

REFERENCES

1. Landy, S.J. and Donnai, D. (1993) Incontinentia Pigmenti (Bloch–Sulzberger syndrome). *J. Med. Genet.*, **30**, 53–59.
2. Scheuerle, A. and Ursini, M.V. (2010) Incontinentia Pigmenti. In Pagon, R.A., Bird, T.D., Dolan, C.R. and Stephens, K. (eds), *GeneReviews*, University of Washington, Seattle (WA), pp. 1993–1999.
3. Fusco, F., Pescatore, A., Bal, E., Ghoul, A., Paciolla, M., Lioi, M.B., D'Urso, M., Rabia, S.H., Bodemer, C., Bonnefont, J.P. *et al.* (2008) Alterations of the IKBKG locus and diseases: an update and a report of 13 novel mutations. *Hum. Mutat.*, **29**, 595–604.
4. Yamaoka, S., Courtois, G., Bessia, C., Whiteside, S.T., Weil, R., Agou, F., Kirk, H.E., Kay, R.J. and Israel, A. (1998) Complementation cloning of NEMO, a component of the IkappaB kinase complex essential for NF-kappaB activation. *Cell*, **93**, 1231–1240.
5. Hayden, M.S. and Ghosh, S. (2004) Signaling to NF-kappaB. *Genes Dev.*, **18**, 2195–2224.
6. Schmidt-Supprian, M., Bloch, W., Courtois, G., Addicks, K., Israel, A., Rajewsky, K. and Pasparakis, M. (2000) NEMO/IKK gamma-deficient mice model Incontinentia Pigmenti. *Mol. Cell.*, **5**, 981–992.
7. Makris, C., Godfrey, V.L., Krahn-Senftleben, G., Takahashi, T., Roberts, J.L., Schwarz, T., Feng, L., Johnson, R.S. and Karin, M. (2000) Female mice heterozygous for IKK gamma/NEMO deficiencies develop a dermatopathy similar to the human X-linked disorder Incontinentia Pigmenti. *Mol. Cell.*, **5**, 969–979.
8. Nelson, D.L. (2006) NEMO, NFkappaB signaling and Incontinentia Pigmenti. *Curr. Opin. Genet. Dev.*, **16**, 282–288.
9. Fusco, F., Bardaro, T., Fimiani, G., Mercadante, V., Miano, M.G., Falco, G., Israel, A., Courtois, G., D'Urso, M. and Ursini, M.V. (2004) Molecular analysis of the genetic defect in a large cohort of IP patients and identification of novel NEMO mutations interfering with NF-kappaB activation. *Hum. Mol. Genet.*, **13**, 1763–1773.
10. Gautheron, J., Pescatore, A., Fusco, F., Esposito, E., Yamaoka, S., Agou, F., Ursini, M.V. and Courtois, G. (2010) Identification of a new NEMO/TRAF6 interface affected in Incontinentia Pigmenti pathology. *Hum. Mol. Genet.*, **19**, 3138–3149.
11. Franze, A., Ferrante, M.I., Fusco, F., Santoro, A., Sanzari, E., Martini, G. and Ursini, M.V. (1998) Molecular anatomy of the human glucose 6-phosphate dehydrogenase core promoter. *FEBS Lett.*, **437**, 313–318.
12. Galgoczy, P., Rosenthal, A. and Platzer, M. (2001) Human–mouse comparative sequence analysis of the NEMO gene reveals an alternative promoter within the neighboring G6PD gene. *Gene*, **271**, 93–98.
13. Fusco, F., Mercadante, V., Miano, M.G. and Ursini, M.V. (2006) Multiple regulatory regions and tissue-specific transcription initiation mediate the expression of NEMO/IKKgamma gene. *Gene*, **383**, 99–107.
14. Martini, G. and Ursini, M.V. (1996) A new lease of life for an old enzyme. *Bioessays*, **18**, 631–637.
15. Vulliamy, T., Beutler, E. and Luzzatto, L. (1993) Variants of glucose-6-phosphate dehydrogenase are due to missense mutations spread throughout the coding region of the gene. *Hum. Mutat.*, **2**, 159–167.
16. Luzzatto, L. (2006) Glucose 6-phosphate dehydrogenase deficiency: from genotype to phenotype. *Haematologica*, **91**, 1303–1306.
17. Cappellini, M.D. and Fiorelli, G. (2008) Glucose-6-phosphate dehydrogenase deficiency. *Lancet*, **371**, 64–74.
18. Aradhya, S., Bardaro, T., Galgoczy, P., Yamagata, T., Esposito, T., Patlan, H., Ciccodicola, A., Munnich, A., Kenwrick, S., Platzer, M. *et al.* (2001) Multiple pathogenic and benign genomic rearrangements occur at a 35 kb duplication involving the NEMO and LAGE2 genes. *Hum. Mol. Genet.*, **10**, 2557–2567.
19. Fusco, F., Paciolla, M., Pescatore, A., Lioi, M.B., Ayuso, C., Faravelli, F., Gentile, M., Zollino, M., D'Urso, M., Miano, M.G. *et al.* (2009) Microdeletion/duplication at the Xq28 IP locus causes a *de novo* IKBKG/NEMO/IKKgamma exon4_10 deletion in families with Incontinentia Pigmenti. *Hum. Mutat.*, **30**, 1284–1291.
20. Vandewalle, J., Van Esch, H., Govaerts, K., Verbeeck, J., Zweier, C., Madrigal, I., Mila, M., Pijkels, E., Fernandez, I., Kohlhase, J. *et al.* (2009) Dosage-dependent severity of the phenotype in patients with mental retardation due to a recurrent copy-number gain at Xq28 mediated by an unusual recombination. *Am. J. Hum. Genet.*, **85**, 809–822.
21. Fusco, F., D'Urso, M., Miano, M.G. and Ursini, M.V. (2010) The LCR at the IKBKG locus is prone to recombine. *Am. J. Hum. Genet.*, **86**, 650–652; author reply 652–653.
22. Vissers, L.E., Bhatt, S.S., Janssen, I.M., Xia, Z., Lalani, S.R., Pfundt, R., Derwinska, K., de Vries, B.B., Gilissen, C., Hoischen, A. *et al.* (2009) Rare pathogenic microdeletions and tandem duplications are microhomology-mediated and stimulated by local genomic architecture. *Hum. Mol. Genet.*, **18**, 3579–3593.
23. Vissers, L.E., Veltman, J.A., van Kessel, A.G. and Brunner, H.G. (2005) Identification of disease genes by whole genome CGH arrays. *Hum. Mol. Genet.*, **14**, R215–R223.
24. Shaw, C.J. and Lupski, J.R. (2004) Implications of human genome architecture for rearrangement-based disorders: the genomic basis of disease. *Hum. Mol. Genet.*, **13**, R57–R64.
25. Pearson, C.E., Nichol Edamura, K. and Cleary, J.D. (2005) Repeat instability: mechanisms of dynamic mutations. *Nat. Rev. Genet.*, **6**, 729–742.
26. Lobachev, K.S., Rattray, A. and Narayanan, V. (2007) Hairpin- and cruciform-mediated chromosome breakage: causes and consequences in eukaryotic cells. *Front. Biosci.*, **12**, 4208–4220.
27. Wells, R.D. (2007) Non-B DNA conformations, mutagenesis and disease. *Trends Biochem. Sci.*, **32**, 271–278.
28. Argueso, J.L., Westmoreland, J., Mieczkowski, P.A., Gawel, M., Petes, T.D. and Resnick, M.A. (2008) Double-strand breaks associated with repetitive DNA can reshape the genome. *Proc. Natl Acad. Sci. USA*, **105**, 11845–11850.
29. Voineagu, I., Narayanan, V., Lobachev, K.S. and Mirkin, S.M. (2008) Replication stalling at unstable inverted repeats: interplay between DNA hairpins and fork stabilizing proteins. *Proc. Natl Acad. Sci. USA*, **105**, 9936–9941.
30. Zhang, F., Seeman, P., Liu, P., Weterman, M.A., Gonzaga-Jauregui, C., Towne, C.F., Batish, S.D., De Vriendt, E., De Jonghe, P., Rautenstrauss, B. *et al.* (2010) Mechanisms for nonrecurrent genomic rearrangements associated with CMT1A or HNPP: rare CNVs as a cause for missing heritability. *Am. J. Hum. Genet.*, **86**, 892–903.
31. Benson, G. (1999) Tandem repeats finder: a program to analyze DNA sequences. *Nucleic Acids Res.*, **27**, 573–580.
32. Chen, J.M., Cooper, D.N., Chuzhanova, N., Ferec, C. and Patrinos, G.P. (2007) Gene conversion: mechanisms, evolution and human disease. *Nat. Rev. Genet.*, **8**, 762–775.
33. Wiese, C., Pierce, A.J., Gauny, S.S., Jasin, M. and Kronenberg, A. (2002) Gene conversion is strongly induced in human cells by double-strand breaks and is modulated by the expression of BCL-x(L). *Cancer Res.*, **62**, 1279–1283.
34. Leduc, F., Maquennehan, V., Nkoma, G.B. and Boissonneault, G. (2008) DNA damage response during chromatin remodeling in elongating spermatids of mice. *Biol. Reprod.*, **78**, 324–332.
35. Srivastava, N. and Raman, M.J. (2007) Homologous recombination-mediated double-strand break repair in mouse testicular extracts and comparison with different germ cell stages. *Cell Biochem. Funct.*, **25**, 75–86.
36. Lander, E.S., Linton, L.M., Birren, B., Nusbaum, C., Zody, M.C., Baldwin, J., Devon, K., Dewar, K., Doyle, M., FitzHugh, W. *et al.* (2001) Initial sequencing and analysis of the human genome. *Nature*, **409**, 860–921.
37. Bacolla, A. and Wells, R.D. (2004) Non-B DNA conformations, genomic rearrangements, and human disease. *J. Biol. Chem.*, **279**, 47411–47414.
38. Matejas, V., Huehne, K., Thiel, C., Sommer, C., Jakubiczka, S. and Rautenstrauss, B. (2006) Identification of Alu elements mediating a partial PMP22 deletion. *Neurogenetics*, **7**, 119–126.
39. Pistorius, S., Gorgens, H., Plaschke, J., Hoehl, R., Kruger, S., Engel, C., Saeger, H.D. and Schackert, H.K. (2007) Genomic rearrangements in MSH2, MLH1 or MSH6 are rare in HNPCC patients carrying point mutations. *Cancer Lett.*, **248**, 89–95.
40. Kolomietz, E., Meyn, M.S., Pandita, A. and Squire, J.A. (2002) The role of Alu repeat clusters as mediators of recurrent chromosomal aberrations in tumors. *Genes Chromosomes Cancer*, **35**, 97–112.
41. Woodward, K.J., Cundall, M., Sperle, K., Sistermans, E.A., Ross, M., Howell, G., Gribble, S.M., Burford, D.C., Carter, N.P., Hobson, D.L. *et al.* (2005) Heterogeneous duplications in patients with Pelizaeus-Merzbacher disease suggest a mechanism of coupled homologous and nonhomologous recombination. *Am. J. Hum. Genet.*, **77**, 966–987.
42. Lee, J.A., Inoue, K., Cheung, S.W., Shaw, C.A., Stankiewicz, P. and Lupski, J.R. (2006) Role of genomic architecture in PLP1 duplication causing Pelizaeus-Merzbacher disease. *Hum. Mol. Genet.*, **15**, 2250–2265.

43. Potocki, L., Bi, W., Treadwell-Deering, D., Carvalho, C.M., Eifert, A., Friedman, E.M., Glaze, D., Krull, K., Lee, J.A., Lewis, R.A. *et al.* (2007) Characterization of Potocki–Lupski syndrome (dup(17)(p11.2p11.2)) and delineation of a dosage-sensitive critical interval that can convey an autism phenotype. *Am. J. Hum. Genet.*, **80**, 633–649.
44. Lee, J.A., Carvalho, C.M. and Lupski, J.R. (2007) A DNA replication mechanism for generating nonrecurrent rearrangements associated with genomic disorders. *Cell*, **131**, 1235–1247.
45. Meloni, T., Forteleoni, G. and Meloni, G.F. (1992) Marked decline of favism after neonatal glucose-6-phosphate dehydrogenase screening and health education: the northern Sardinian experience. *Acta Haematol.*, **87**, 29–31.
46. Filosa, S., Giacometti, N., Wangwei, C., De Mattia, D., Pagnini, D., Alfinito, F., Schettini, F., Luzzatto, L. and Martini, G. (1996) Somatic-cell selection is a major determinant of the blood-cell phenotype in heterozygotes for glucose-6-phosphate dehydrogenase mutations causing severe enzyme deficiency. *Am. J. Hum. Genet.*, **59**, 887–895.
47. Longo, L., Vanegas, O.C., Patel, M., Rosti, V., Li, H., Waka, J., Merghoub, T., Pandolfi, P.P., Notaro, R., Manova, K. *et al.* (2002) Maternally transmitted severe glucose 6-phosphate dehydrogenase deficiency is an embryonic lethal. *EMBO J.*, **21**, 4229–4239.
48. Parrish, J.E., Scheuerle, A.E., Lewis, R.A., Levy, M.L. and Nelson, D.L. (1996) Selection against mutant alleles in blood leukocytes is a consistent feature in Incontinentia Pigmenti type 2. *Hum. Mol. Genet.*, **5**, 1777–1783.
49. Yoshida, N., Abe, H., Ohkuri, T., Wakita, D., Sato, M., Noguchi, D., Miyamoto, M., Morikawa, T., Kondo, S., Ikeda, H. *et al.* (2006) Expression of the MAGE-A4 and NY-ESO-1 cancer-testis antigens and T cell infiltration in non-small cell lung carcinoma and their prognostic significance. *Int. J. Oncol.*, **28**, 1089–1098.
50. Nenci, A., Huth, M., Funteh, A., Schmidt-Supprian, M., Bloch, W., Metzger, D., Chambon, P., Rajewsky, K., Krieg, T., Haase, I. *et al.* (2006) Skin lesion development in a mouse model of Incontinentia Pigmenti is triggered by NEMO deficiency in epidermal keratinocytes and requires TNF signaling. *Hum. Mol. Genet.*, **15**, 531–542.
51. Sebban, H. and Courtois, G. (2006) NF-kappaB and inflammation in genetic disease. *Biochem. Pharmacol.*, **72**, 1153–1160.
52. Lupski, J.R. (1998) Genomic disorders: structural features of the genome can lead to DNA rearrangements and human disease traits. *Trends Genet.*, **14**, 417–422.
53. Bardaro, T., Falco, G., Sparago, A., Mercadante, V., Gean Molins, E., Tarantino, E., Ursini, M.V. and D'Urso, M. (2003) Two cases of misinterpretation of molecular results in Incontinentia Pigmenti, and a PCR-based method to discriminate NEMO/IKKgamma gene deletion. *Hum. Mutat.*, **21**, 8–11.
54. Fimiani, G., Laperuta, C., Falco, G., Ventruto, V., D'Urso, M., Ursini, M.V. and Miano, M.G. (2006) Heterozygosity mapping by quantitative fluorescent PCR reveals an interstitial deletion in Xq26.2-q28 associated with ovarian dysfunction. *Hum. Reprod.*, **21**, 529–535.
55. Pellegrini, G., Ranno, R., Stracuzzi, G., Bondanza, S., Guerra, L., Zambruno, G., Micali, G. and De Luca, M. (1999) The control of epidermal stem cells (holoclones) in the treatment of massive full-thickness burns with autologous keratinocytes cultured on fibrin. *Transplantation*, **68**, 868–879.
56. Tseng, H. and Green, H. (1994) Association of basonuclin with ability of keratinocytes to multiply and with absence of terminal differentiation. *J. Cell. Biol.*, **126**, 495–506.
57. D'Anna, F., De Luca, M., Cancedda, R., Zicca, A. and Franzi, A.T. (1988) Elutriation of human keratinocytes and melanocytes from *in vitro* cultured epithelium. *Hystochem. J.*, **20**, 674–678.
58. Nylander, K., Vojtesek, B., Nenutil, R., Lindgren, B., Roos, G., Zhanxiang, W., Sjostrom, B., Dahlqvist, A. and Coates, P.J. (2002) Differential expression of p63 isoforms in normal tissues and neoplastic cells. *J. Pathol.*, **198**, 417–427.
59. Laurikkala, J., Mikkola, M.L., James, M., Tummers, M., Mills, A.A. and Thesleff, I. (2006) p63 regulates multiple signalling pathways required for ectodermal organogenesis and differentiation. *Development*, **133**, 1553–1563.